

The velocity distribution of barotropic turbulence

Annalisa Bracco^{a)}

Istituto di Cosmogeofisica del CNR, Torino, Italy

Joe LaCasce

Woods Hole Oceanographic Institution, Woods Hole, Massachusetts

Claudia Pasquero and Antonello Provenzale

Istituto di Cosmogeofisica del CNR, Torino, Italy

(Received 11 January 2000; accepted 19 June 2000)

We study the statistical properties of the velocity and velocity gradient distributions in barotropic turbulence. At large enough Reynolds number, the velocity distribution becomes non-Gaussian outside the vortex cores, and its characteristics are completely determined by the properties of the far field induced by the coherent vortices. The velocity gradients are always non-Gaussian inside coherent vortices, due to the spatial velocity correlations associated with the ordered flow in the vortex cores, and become non-Gaussian also in the background turbulence at large enough Reynolds number. © 2000 American Institute of Physics. [S1070-6631(00)51110-6]

I. INTRODUCTION

A classic approach to the study of turbulent geophysical flows is based on a statistical description.¹ Stochastic models used to describe particle transport in large Reynolds number flows usually consider only the first- and second-order moments (i.e., mean and variance) and rely upon the hypothesis of Gaussian velocities.² For Gaussian distributions, the higher-order moments, needed to define statistical quantities such as the minimum or maximum time tracers take to reach a given location, can be derived from the mean and the variance.

On the other hand, numerical and theoretical studies of point-vortex systems and two-dimensional turbulence,³⁻⁵ laboratory experiments,⁶ and analyses of subsurface floats in the ocean⁷ indicate that velocity distributions in rotating turbulent flows can be non-Gaussian. In this case, higher-order moments cannot be derived from the mean and the variance and the knowledge of the full shape of the velocity distribution becomes overly important for properly formulating stochastic dispersion models.⁸

To explore this issue in a simple but realistic model, here we analyze in some detail a set of numerical simulations of the dynamics of rotating barotropic fluids under the quasigeostrophic approximation. This model, usually referred to as barotropic turbulence, is a first approximation to the description of the dynamics of large-scale geophysical flows.^{9,10} Barotropic turbulence is dominated by the presence of coherent vortices, and it has been shown to be characterized by a non-Gaussian velocity distribution.³ Here we study the dependence of the velocity and velocity gradient distributions on the Reynolds number and we further elucidate the

dynamical origin of the non-Gaussian behavior.

The rest of the paper is organized as follows. In Sec. II we introduce the equation of motion for barotropic turbulence and the numerical scheme we use to solve it. In Sec. III we discuss the results of the analysis of the simulated velocity fields, investigating the role of Reynolds number, initial conditions, and viscosity. A non-Gaussian velocity distribution is found whenever the Reynolds number is large enough. Here we also analyze the velocity distributions in regions with different dynamical properties, showing that non-Gaussian distributions are observed mainly outside coherent structures. In Sec. IV the role of the vortices is explored in detail. We show that the background velocity field can be separated into a contribution due to the far field of the vortices and a contribution generated by the local vorticity in regions far from the vortices. In Sec. V the example of point-vortex systems is considered. In the conclusion section, we briefly consider how free-surface effects and differential rotation affect the velocity distribution, and we discuss the possible implications of these results on the interpretation of velocity pdfs in the ocean.

II. DYNAMICS OF BAROTROPIC TURBULENCE

The equation of motion for barotropic turbulence in the quasigeostrophic approximation is

$$\frac{Dq}{Dt} = \frac{\partial q}{\partial t} + [\psi, q] = D, \quad (1)$$

where D/Dt is the total advective derivative, $[\psi, q] = \partial_x \psi \partial_y q - \partial_y \psi \partial_x q$ is the two-dimensional Jacobian operator, D is a generic dissipative term, ψ is the streamfunction, and $q = \omega + f - \psi/R^2$ is potential vorticity. Here, f is the Coriolis parameter and $R = R_0/L$, where $R_0 = \sqrt{gH}/f_0$ is the dimensional Rossby deformation radius and L is the size of the domain considered.

^{a)} Author to whom correspondence should be addressed. Istituto di Cosmogeofisica del CNR di Torino, C.so Fiume 4, 10133, Italy. Electronic mail: annalisa@icg.to.infn.it; fax: +39 011 6604056; phone: +39 011 6306806.

In this approximation, relative vorticity is defined as $\omega = \nabla^2 \psi$. Consistently, the velocity field $\mathbf{u} = (u, v)$ is given by $u = -\partial_y \psi$ and $v = \partial_x \psi$. On a spherical planet, the Cartesian reference frame (x, y) is defined on the plane of motion such that the variable x refers to longitudinal variations and y varies with latitude.

The Coriolis parameter f in the β -plane approximation becomes $f = f_0 + \beta y$, where $f_0 = 2\Omega \sin \theta_0$, Ω is the rotation frequency of the Earth, and θ_0 is a reference latitude. Differential rotation (i.e., the variation of the Coriolis parameter with latitude) enters as a linear correction through the parameter $\beta = 2\Omega \cos \theta_0 / R_E$, where R_E is the radius of the Earth.

The last term in the definition of potential vorticity is usually referred to as the free-surface contribution, and it is written in terms of the dimensionless Rossby deformation radius. When the domain is sufficiently small, free-surface effects and the variation of the Coriolis parameter with latitude can be discarded. In this case, potential vorticity can be replaced by relative vorticity in Eq. (1). We first consider this approximation, and, in the discussion section, we briefly discuss how the results are modified by the inclusion of free-surface effects and differential rotation.

The dissipative term D represents either molecular or eddy viscosity. In the latter case it is considered as a parametrization of unresolved small-scale motions. Here we use the general form

$$D = (-1)^{n-1} \nu_n \nabla^{2n} \psi, \tag{2}$$

where ν_n is the viscosity coefficient and n is a positive integer. For $n = 1$, D is standard Newtonian viscosity, while for $n > 1$, D represents the so-called hyperviscosity.

In the inviscid case ($D = 0$), Eq. (1) has an infinite number of conserved quantities. Among these, there are two quadratic invariants: the mean energy E and the mean enstrophy Z , given by

$$E = \frac{1}{2L^2} \int (\nabla \psi)^2 dx dy, \tag{3}$$

$$Z = \frac{1}{2L^2} \int (\nabla^2 \psi)^2 dx dy, \tag{4}$$

where L is the size of the (square) domain.

The simultaneous conservation of these two quantities leads to a direct cascade of enstrophy toward small scales, and an inverse cascade of energy from small to large scales. The term responsible for the energy and enstrophy transfers is the only nonlinear term in Eq. (1), i.e., the Jacobian term.

In the dissipative case, spectral transfers are present as well, even if energy and enstrophy are decaying. These spectral transfers lead to the development of long-lived coherent structures, as revealed by numerical simulations¹¹ and laboratory experiments.¹² In general, coherent vortices can be defined as approximately axisymmetrical vorticity concentrations whose lifetime is much larger than their eddy turnover time. The vortices play an especially important role in tracer dynamics, due to their capability of trapping passive tracers for long times and transporting them over large distances (see, e.g., Provenzale¹³ for a review).

The identification of the different regions present in the field can be done in several ways. The simplest, and more naive, criterion identifies coherent structures as regions where the vorticity $\omega(x, y)$ exceeds a given threshold value. Despite its coarseness, this criterion has largely and profitably been used in the literature^{14,15} due to its simplicity. Other criteria seek for approximately circular connected domains of high vorticity around a central peak,¹⁶ or employ wavelet-based classification schemes.¹⁷⁻¹⁹

A different approach has been proposed by Okubo²⁰ and Weiss,²¹ and recently improved by Hua and Klein.²² This criterion is based on the use of the quantity $Q(x, y, t) = S^2 - \omega^2$, which measures the relative contribution of the squared vorticity ω^2 and of the squared strain S^2 . The latter is defined as $S^2 = s_n^2 + s_s^2$, where $s_n = \partial_x u - \partial_y v$ and $s_s = \partial_y u + \partial_x v$ are, respectively, the normal and shear components of strain. Regions dominated by rotation have negative values of Q and are referred to as elliptic domains, while hyperbolic domains have $Q > 0$ and are characterized by strong deformation. Vortex cores are associated with strongly negative values of Q .

In the following, we integrate the vorticity equation (1) starting from random, Gaussian initial conditions. The integration of the equation of motion is performed by a standard pseudospectral code with $\frac{2}{3}$ dealiasing and a third-order Adams–Bashforth time integration scheme in a doubly periodic square domain with size $L = 2\pi$. The resolution of the doubly periodic domain has been varied from 512×512 to 1024×1024 collocation points.

We consider two types of initial energy spectra that have been used in the literature. One is a narrow-band (NB) spectrum¹⁶ given by

$$E_{\text{NB}}(k) = \frac{E_0 k^6}{\left(1 + \frac{k}{60}\right)^{18}}, \tag{5}$$

and the other is a broadband (BB) spectrum²³ given by

$$E_{\text{BB}}(k) = \frac{E_0 k}{\left(1 + \frac{k^4}{6}\right)}. \tag{6}$$

Figure 1 and 2 show the vorticity fields at time $t = 15$ generated using a biharmonic viscosity operator ($n = 2$) and broadband initial energy spectrum with $\nu_2 = 5 * 10^{-8}$ (Fig. 1) and narrow-band spectrum with $\nu_2 = 5 * 10^{-9}$ [Fig. 2(a)], or $\nu_2 = 5 * 10^{-7}$ [Fig. 2(b)].

III. VELOCITY AND VELOCITY GRADIENT DISTRIBUTIONS

We next consider the shape of the distribution of velocities and velocity gradients, and its dependence on the Reynolds number and the initial vorticity spectrum.

In Fig. 3(a) we show the velocity pdf of the turbulent field displayed in Fig. 2(a) for $t = 15$. The mean eddy turnover time at $t = 15$ is $T_E = 0.17$, for comparison, $T_E = Z^{-1/2} = 0.12$ at time $t = 0$. Since the velocity field is statistically isotropic and has zero average, we have considered the distribution of the modulus of the two components, normalized

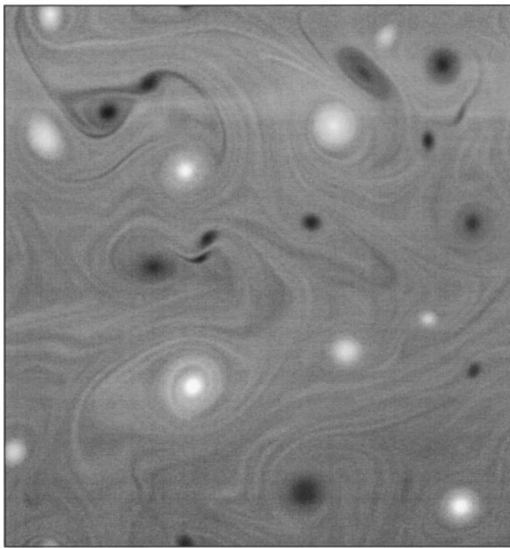


FIG. 1. Vorticity field at time $t=15$, as given by numerical simulation of Eq. (1) with $1/R=0$, $\beta=0$, and a biharmonic dissipation term with $\nu_2=5 \times 10^{-8}$. The resolution is 512×512 grid points and the initial conditions are given by a random vorticity field with a broadband energy spectrum.

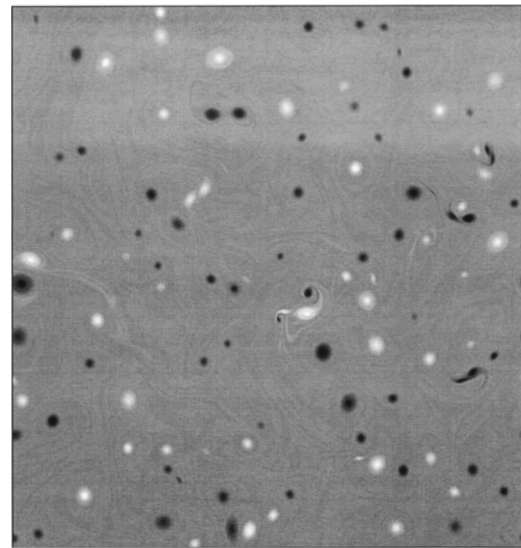
by the velocity rms value. Figure 3(a) clearly indicates that there is significant deviation from a Gaussian distribution, as already discussed by Jiménez.³

When lowering the Reynolds number, however, the departure from Gaussianity is reduced and it disappears at low Re. In Fig. 3(b) we show the velocity pdf of the turbulent field displayed in Fig. 2(b) for $t=15$. In this case, the mean eddy turnover time is $T_E=0.57$ at $t=15$ and the distribution is indistinguishable from a Gaussian. Simulations at intermediate values of the Reynolds number have revealed a smooth transition from Gaussian behavior at small Re toward non-Gaussian pdfs at high Re, as indicated, for example, by a gradual increase of the kurtosis for growing Re.

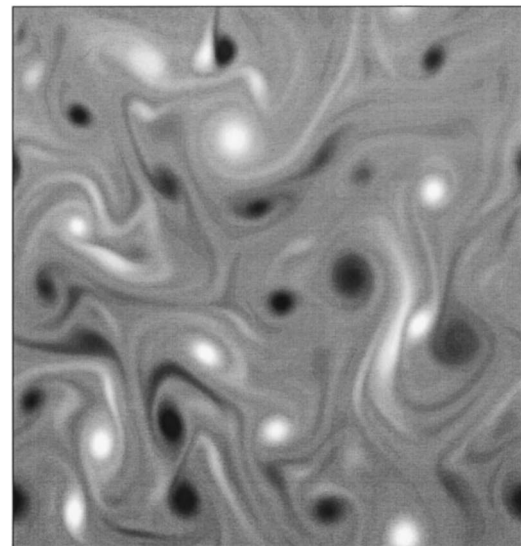
The above results do not depend on the specific dissipation scheme that is employed. A simulation performed with higher resolution (1024×1024 grid points) and Newtonian viscosity with $n=1$ and $\nu_1=5 \times 10^{-5}$, has a global evolution comparable with that with $n=2$ and $\nu_2=5 \times 10^{-8}$, and produces similar non-Gaussian pdfs. Another simulation, performed with a higher-order viscosity operator ($D=10^{-16} \nabla^8 \omega$), confirms that pdfs at high Reynolds numbers are strongly non-Gaussian, independent of the order n of hyperviscosity chosen.

On the other hand, the shape of the velocity pdf does depend on the initial conditions. When we change the shape of the initial energy spectrum to a broad band form, keeping the dissipation unchanged, the departure from a Gaussian distribution is reduced. For the broad spectrum peaked at large scales, Eq. (6), the pdf is well described by a Gaussian, and the use of different viscosity coefficients does not lead to any significant deviation from Gaussianity.

To summarize the results found in the simulations, in Table I we report the kurtosis $k=\langle u^4 \rangle / \langle u^2 \rangle^2$ of the velocity distributions for the different cases considered. The value $k=3$ characterizes a Gaussian distribution, while higher values are associated with the presence of non-Gaussian tails.



(a)



(b)

FIG. 2. (a) Vorticity field at time $t=15$, for a narrow-band initial energy spectrum at high Re ($\nu_2=5 \times 10^{-9}$). (b) Vorticity field for the same initial conditions at lower Re ($\nu_2=5 \times 10^{-7}$).

The Kolmogorov–Smirnov (K–S) test, which measures the significance of the maximum deviation between an empirical and a specified theoretical distribution, has been used to quantify the departure from a Gaussian. Low values of the K–S statistic (i.e., $\alpha \leq 0.05$ in the table) indicate rejection of the null hypothesis of a Gaussian distribution at the 95% confidence level. Thus, non-Gaussian velocity pdfs seem to emerge only for narrow-band initial conditions when the Reynolds number is large enough.

The next step is to determine whether there are significant differences in the distributions associated with the different topological domains of two-dimensional (2-D) turbulence, as suggested by Bracco *et al.*⁷ To address this issue, we partition the turbulent field into three different regions, as discussed by Elhmaïdi *et al.*²⁴ Vortex cores are identified as regions where Q is strongly negative and the modulus of the

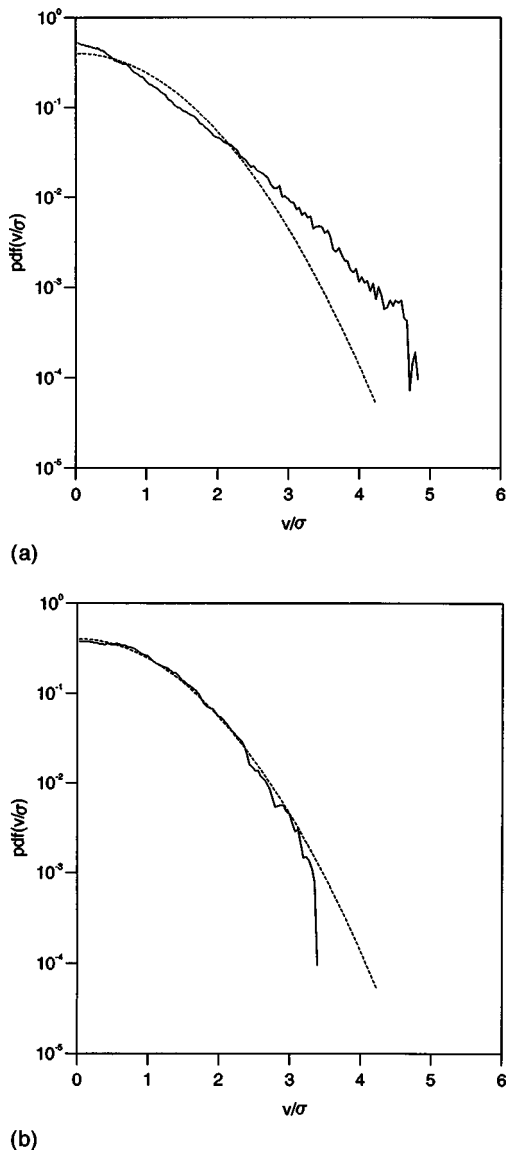


FIG. 3. One-point velocity distribution for the fields shown in Fig. 2(a) (panel a) and in Fig. 2(b) (panel b). The dashed line in each panel shows a Gaussian distribution with the same variance of the data.

vorticity is larger than a fixed threshold ω_V , chosen as in Benzi *et al.*¹⁴ as $\omega_V=0.2\sigma_\omega$, where σ_ω is the standard deviation of the vorticity field. Circulation cells are identified as regions where Q attains large positive values and the kinetic energy is large. Then, what is left is the background, where $Q \approx 0$ and the energy is low. Figure 4 shows the velocity pdfs for the vortex cores [panel (a)], for the region outside vortices [i.e., circulation cells and background, panel (b)], and for the background alone [panel (c)] in the case of narrow-band initial conditions and high Reynolds number. The results do not significantly change if other similar threshold values are chosen. Inside vortices, the distribution is nearly Gaussian. A different result is obtained for the velocity distribution in the region outside the vortices. Here, the velocity distribution has both a high tail for large velocities and a non-Gaussian central portion at small velocities, indicating that deviations from normality are not simply due to energetic events. The further exclusion of the velocities in the circulation cells around the vortices (where large velocities are expected²⁴) does not change the non-Gaussian distribution significantly, as shown by the similarity between Figs. 4(b) and 4(c).

In the corresponding analysis performed on the field at low Reynolds number, nearly Gaussian behavior has been found everywhere, independent of the region selected.

Also of interest are the distributions of velocity gradients (and velocity differences). Jiménez³ and Min *et al.*⁴ provided analytic expressions for the distribution of velocity gradients generated by an ensemble of point vortices, and showed that it rapidly converges to a Cauchy distribution when the number of vortices increases. Figure 5 show the distribution of velocity gradients, $\partial u/\partial x$ and $\partial u/\partial y$, for narrow-band initial conditions and the two values of the Reynolds number considered. We could have equivalently considered $\partial v/\partial x$ and $\partial v/\partial y$, due to the isotropy of the field. However, considering the four elements of the velocity Jacobian altogether is redundant, due to the relationships $\partial v/\partial y = -\partial u/\partial x$ and $\partial v/\partial x = \omega + \partial u/\partial y$, that make these quantities dependent on each other. The three curves in each panel refer, respectively,

TABLE I. Results of the analysis of the full set of velocity fields considered in the text. The columns contain, in order, the number of collocation points on each axis, the properties of the initial spectrum [see Eqs. (5) and (6)], the exponent n of the Laplacian, and the viscosity coefficient ν_n [see Eq. (2)], the value of β , and of the nondimensional Rossby deformation radius, the standard deviation σ_{tot} , and the kurtosis k_{tot} of the velocity field and the K-S statistics. In the last two rows, given the anisotropy due to the presence of $\beta \neq 0$, the two components u and v of the velocity field are analyzed separately.

Resolution	i.c	n	ν_n	β	R	σ_{tot}	k_{tot}	α			
512	NB	2	5×10^{-7}	0	0	0.4	3.5	0.19			
512	NB	2	5×10^{-8}	0	0	0.6	4.0	4.9×10^{-3}			
512	NB	2	5×10^{-9}	0	0	0.7	4.3	1.9×10^{-6}			
512	NB	4	1×10^{-16}	0	0	0.7	4.7	5.6×10^{-11}			
1024	NB	1	3×10^{-5}	0	0	0.6	3.7	0.018			
512	BB	2	5×10^{-8}	0	0	0.7	3.3	0.32			
512	NB	4	1×10^{-16}	0	0.25	0.5	5.6	8.7×10^{-10}			
512	NB	2	5×10^{-8}	10	0	0.5	0.7	3.2	2.5	0.18	1.5×10^{-6}
512	NB	2	5×10^{-8}	10	0.25	0.4	0.4	3.3	2.6	3.2×10^{-2}	2.7×10^{-2}

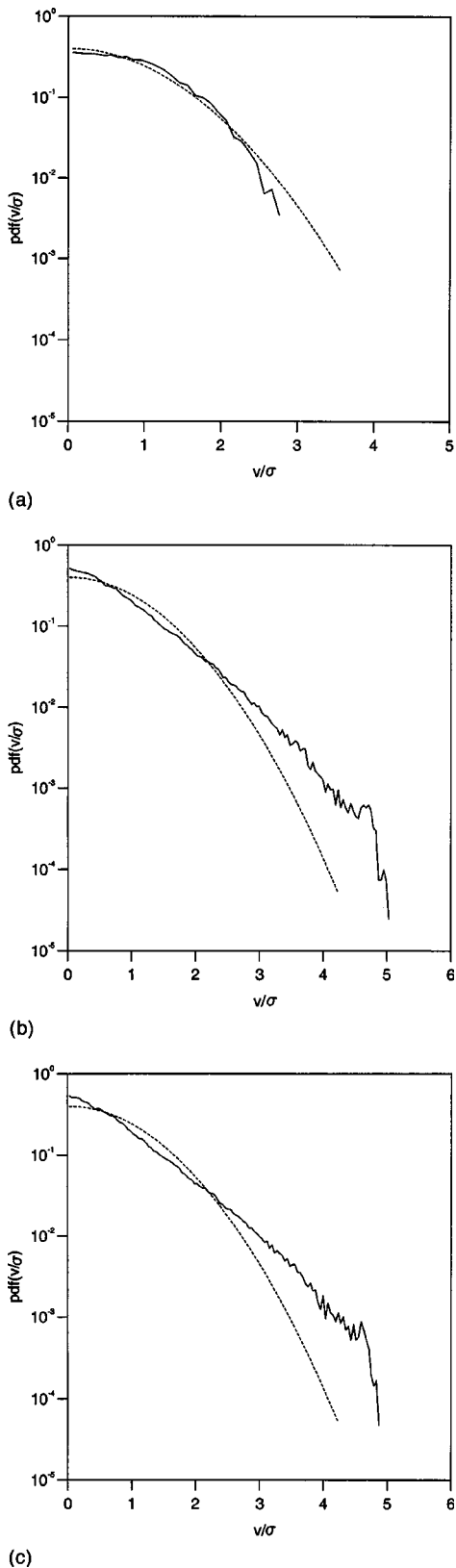


FIG. 4. Velocity pdfs for the vorticity field of Fig. 2(a), as obtained by considering only regions inside vortices (panel a), outside vortices (panel b), and in the background outside vortices and circulation cells (panel c). The dashed line shows a Gaussian distribution with the same variance of the data.

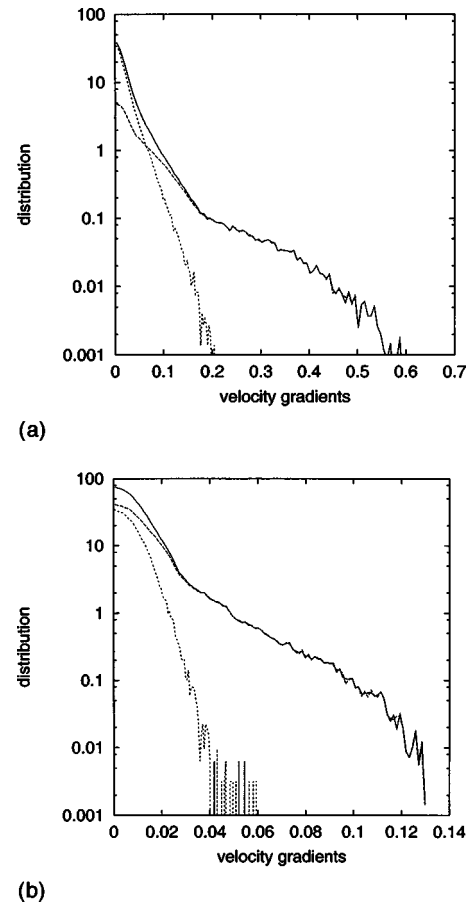


FIG. 5. Panels (a) and (b) show the velocity gradient distribution for the vorticity fields shown, respectively, in Figs. 2(a) and 2(b). In each panel, the solid curve refers to the whole field, the long-dashed curve refers to the velocity gradients inside vortex cores, and the short-dashed curve refers to the velocity gradients outside vortices.

to the velocity gradient pdf in the whole field, in the vortex cores, and in the background. For the whole field, both distributions are non-Gaussian, indicating the presence of significant spatial correlations in the velocity field. This should indeed be expected due to the presence of coherent vortices. We also note that a fit of these pdfs to a Cauchy distribution does not produce satisfactory results, contrary to what occurs for point vortices. This is due to the fact that these vortices have finite cores, that modify the tails of the pdfs at large velocity gradients, and that there is a background turbulent field between the vortices, that affects the central portion of the pdfs at low values of the gradients.

Inside the vortices, the distribution of velocity gradients are both non-Gaussian and they have a similar shape. This indicates that, inside vortices, the ordered nature of the flow induces strong velocity correlations that can be understood in terms of “dressed” point vortex singularities, as discussed by Jiménez³ and Min *et al.*⁴ The situation changes completely outside the vortices, where the dependence on the Reynolds number appears much more clearly. For low Re, the velocity gradients have an approximately Gaussian

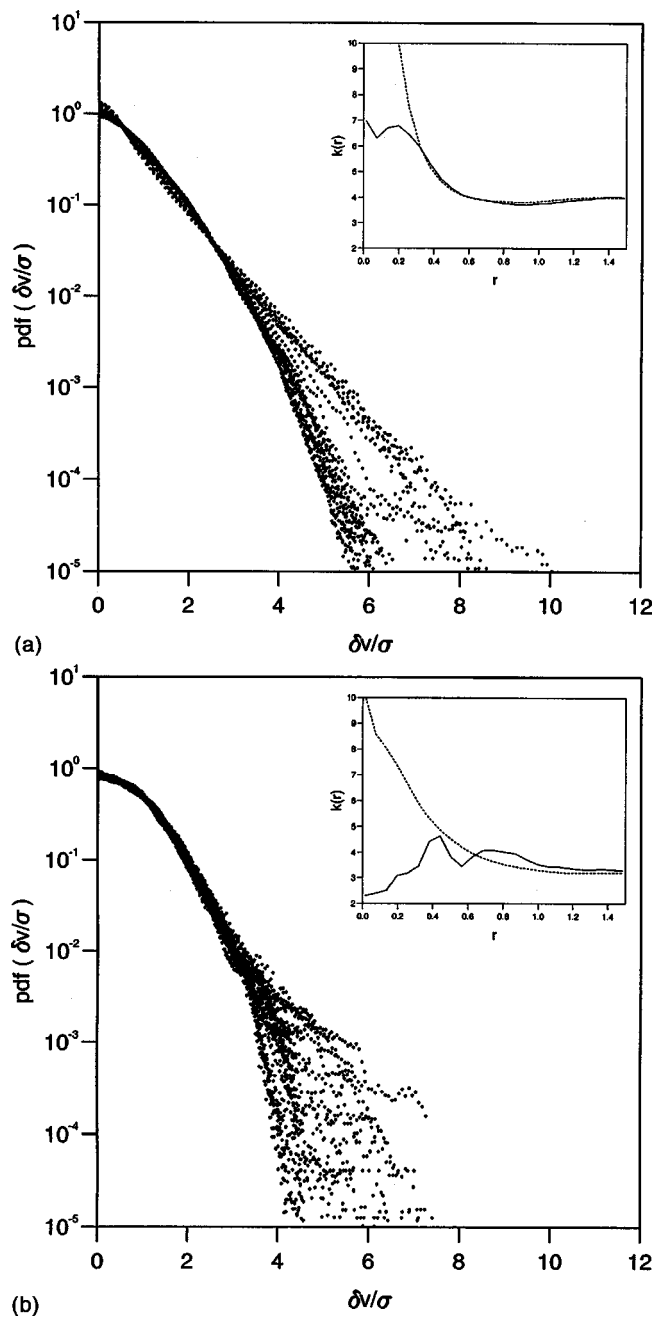


FIG. 6. The distribution of the velocity differences between points at distance r , for the vorticity field of Fig. 2(a) [panel (a)] and Fig. 2(b) [panel (b)]. The distance r varies from 5 to 100 grid points. The insets show the kurtosis versus the distance r for the whole field (dashed line) and for the background (solid line).

distribution in the background. For large Re , the distribution becomes definitely non-Gaussian.

A further confirmation of the anomalous behavior of the velocity field outside vortices, for the high Reynolds number case, comes from the analysis of the distribution of the velocity differences δu between points located at a given distance r . For a random Gaussian velocity distribution with no space correlations, the kurtosis of the velocity differences, $k(r) = \langle \delta u^4 \rangle / \langle \delta u^2 \rangle^2$, assumes the standard value $k=3$ for any distance r . By contrast, space correlations induce higher values of the kurtosis at small scales.²⁵ For both values of the Reynolds number considered here, the presence of vortices induces space correlations. Thus, a value of the kurtosis

larger than 3 at small separations is observed anyway. At high Reynolds number, however, the kurtosis grows as r decreases also outside the vortices [Fig. 6(a)], further confirming the presence of space correlations also in the background turbulence. Conversely, at low Reynolds number the kurtosis does not grow for decreasing separations outside the vortices [Fig. 6(b)], indicating that the space correlations of the velocity field are entirely concentrated inside the vortices.

To summarize the results of this section, we conclude that non-Gaussian velocity and velocity gradient pdfs are observed in regions outside the vortices, for large enough Re

and for narrow-band initial conditions. Inside vortices, the velocity pdfs are approximately Gaussian, while velocity gradients have a non-Gaussian distribution, independently of the value of Re (at least in the range explored here). This latter behavior simply reflects the spatial velocity correlations generated by the ordered (laminar) flow inside the vortex cores.

IV. VORTICES AND BACKGROUND: TWO SEPARATE EFFECTS

In principle, the non-Gaussian behavior of the velocities outside the vortices could be due to both the local properties of the background turbulence, that might develop different characteristics at different Reynolds number, or to a nonlocal effect of the vortices themselves, as suggested by Jiménez.³ In the following, we show that the latter interpretation is the correct one.

To address this issue, we must first separate the contribution of the local properties of the background from that due to the far field of the vortices. As before, vortices are identified as regions where $|\omega| > \omega_v = 0.2\sigma_\omega$. Regions where $|\omega| < \omega_v$ are considered to be the background turbulence and are referred to as \mathcal{B} .

Thus we define two ‘‘clipped’’ fields ω_b and ω_v as

$$\omega_b = \begin{cases} \omega & \text{for } |\omega| < \omega_v, \\ 0 & \text{for } |\omega| \geq \omega_v, \end{cases} \quad (7)$$

$$\omega_v = \begin{cases} 0 & \text{for } |\omega| < \omega_v, \\ \omega & \text{for } |\omega| \geq \omega_v. \end{cases} \quad (8)$$

In this way, the vorticity field ω is partitioned into two separate contributions, $\omega = \omega_b + \omega_v$. The field ω_b does not give any contribution inside vortices, while ω_v does not give any contribution in the background. Thus, we have attained a *local* separation of the vorticity inside and outside the coherent structures. The velocity field, however, is an integral of the vorticity, and the above separation generates nonlocal effects. In particular, the velocity field associated with ω_v is not necessarily concentrated inside vortices and it can give a nonzero contribution also in the background. To see this, we write the vorticity field inside the coherent structures, ω_v , as a Fourier integral, i.e.,

$$\begin{aligned} \omega_v(\mathbf{x}) &= \nabla^2(\psi_v) = \frac{1}{\sqrt{2\pi}} \int \hat{\omega}_v(\mathbf{k}) e^{i\mathbf{k}\cdot\mathbf{x}} d\mathbf{k} \\ &= \begin{cases} \omega(\mathbf{x}) = \frac{1}{\sqrt{2\pi}} \int \hat{\omega}(\mathbf{k}) e^{i\mathbf{k}\cdot\mathbf{x}} d\mathbf{k}, & \text{for } \mathbf{x} \in \nu, \\ 0, & \text{for } \mathbf{x} \in \mathcal{B}, \end{cases} \end{aligned} \quad (9)$$

where $\mathbf{x} = (x, y)$ and $\mathbf{k} = (k_x, k_y)$. When we calculate the velocity field induced by ω_v , we obtain

$$u_v(\mathbf{x}) = -\frac{\partial\psi_v}{\partial y} = \frac{1}{\sqrt{2\pi}} \int -\frac{k_y}{k^2} \hat{\omega}_v(\mathbf{k}) e^{i\mathbf{k}\cdot\mathbf{x}} d\mathbf{k}$$

and

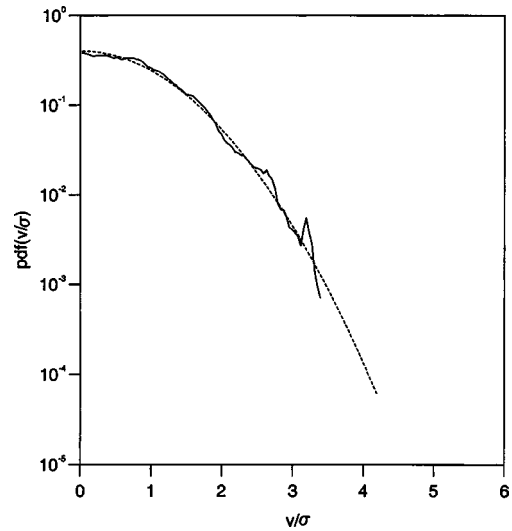


FIG. 7. One-point velocity pdfs of the *background-induced velocity field* for the field of Fig. 2(a). The dashed line shows a Gaussian distribution with the same variance.

$$v_v(\mathbf{x}) = \frac{\partial\psi_v}{\partial x} = \frac{1}{\sqrt{2\pi}} \int \frac{k_x}{k^2} \hat{\omega}_v(\mathbf{k}) e^{i\mathbf{k}\cdot\mathbf{x}} d\mathbf{k}.$$

In general, $\mathbf{u}_v(\mathbf{x}) \neq 0$ even for $\mathbf{x} \in \mathcal{B}$, because the equality $\int \hat{\omega}_v(\mathbf{k}) e^{i\mathbf{k}\cdot\mathbf{x}} d\mathbf{k} = 0$, valid for $\mathbf{x} \in \mathcal{B}$, implies $\int (k_x/k^2) \hat{\omega}_v(\mathbf{k}) e^{i\mathbf{k}\cdot\mathbf{x}} d\mathbf{k} = 0$ only if $\hat{\omega}_v(\mathbf{k}) = 0$ for any given wave number \mathbf{k} , which is not the case.

Thus, the original velocity field \mathbf{u} in the background is due to both \mathbf{u}_b , obtained by removing the vorticity inside the coherent structures, and to the contribution due to the vortices, \mathbf{u}_v .

For this reason, we refer to a *background-induced velocity field* \mathbf{u}_b and to a *vortex-induced velocity field* \mathbf{u}_v , obtained by inverting the Poisson equation for the fields ω_b and ω_v , respectively. Each of the fields is different from the original velocity field both in the background and inside the vortices.

Figures 7 and 8 show the velocity pdfs obtained for the two fields \mathbf{u}_b and \mathbf{u}_v separately. The pdf of the background-induced velocity field is Gaussian, while that of the vortex-induced field is practically coincident with the distribution of the original velocity field, both in the high [Fig. 8(a)] and low [Fig. 8(b)] Reynolds number cases. Completely analogous results are obtained for the velocity gradients. In the background, the kinetic energy associated with \mathbf{u}_b is about 1% that associated with \mathbf{u}_v , indicating that the properties of the velocity field are almost entirely determined by the characteristics of the vortices, not only in regions close to the vortices, but everywhere.

V. THE POINT-VORTEX ANALOGY

The results of the previous sections indicate that non-Gaussian pdfs are found whenever the vortices are small and intense, as obtained for high Reynolds number and narrow-band initial spectra. Conversely, low values of the Reynolds number, and/or broadband initial spectra, lead to larger and less intense vortices²⁶ and to Gaussian velocity pdfs. Thus, the behavior of the velocity distributions seems to be com-

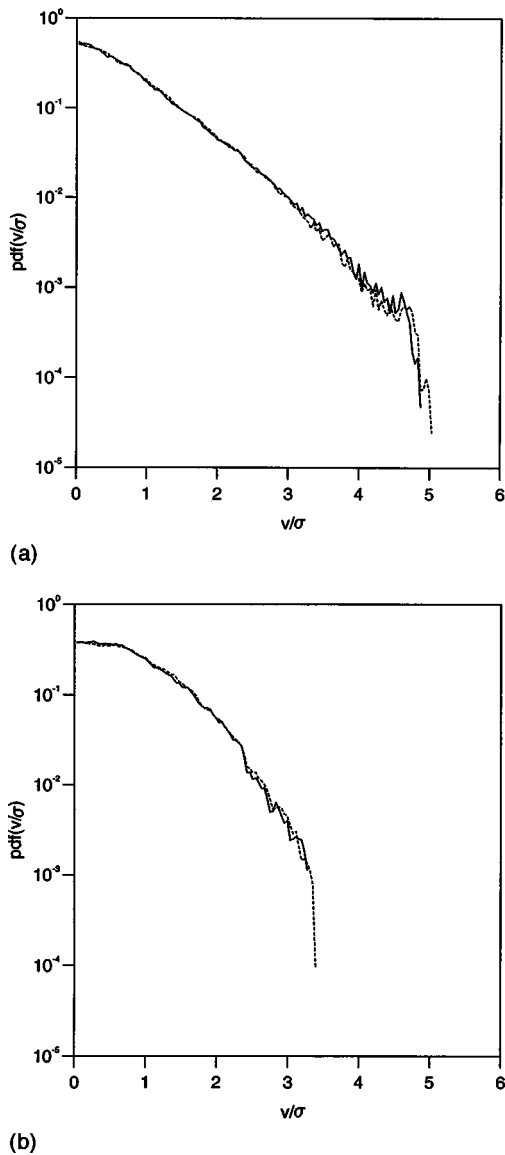


FIG. 8. One-point velocity pdfs of the *vortex-induced velocity field* (solid lines) and of the total velocity field (dashed lines) for the field of Fig. 2(a) [panel (a)] and of Fig. 2(b) [panel (b)].

pletely determined by the vortex population. This naturally suggests resorting to the point-vortex analogy, where the turbulent dynamics is described in terms of the interaction between a finite number of pointwise vorticity concentrations.^{27,26,28}

In this approach, the vorticity field can be written as the sum of the individual vortex contributions (i.e., a singular version of the field ω_v defined in the previous section),

$$\omega(\mathbf{x}, t) = \sum_{i=1}^N \Gamma_i \delta[\mathbf{x} - \mathbf{x}_i(t)],$$

where Γ_i is the circulation of the i vortex, located at position $\mathbf{x}_i(t)$, and the sum is performed over the total number N of point vortices. The equations of motion of the point-vortex system can be cast in Hamiltonian form,

$$\Gamma_i \frac{dx_i}{dt} = \frac{\partial H}{\partial y_i}, \quad \Gamma_i \frac{dy_i}{dt} = -\frac{\partial H}{\partial x_i},$$

where H is the Hamiltonian of the system,

$$H(\{\mathbf{x}_i\}) = -\sum_{i \neq j} \frac{\Gamma_i \Gamma_j}{2} G(\mathbf{x}_i, \mathbf{x}_j). \tag{10}$$

The explicit form of the Green's function, G , depends on the boundary conditions. In a doubly periodic domain with length $[2\pi, 2\pi]$, G takes the form²⁸

$$G(\mathbf{x}_i, \mathbf{x}_j) = \sum_{m=-\infty}^{\infty} \ln \left[\frac{\cosh(x_i - x_j - 2\pi m) - \cos(y_i - y_j)}{\cosh 2\pi m} \right] - \frac{(x_i - x_j)^2}{2\pi}. \tag{11}$$

The statistical properties of the velocity field generated by a point-vortex system have been studied by Jiménez,³ Min *et al.*,⁴ and Weiss *et al.*⁵

If there is only one vortex, the modulus U of the velocity, $U = (u^2 + v^2)^{1/2}$, at a point at distance r from it is proportional to $1/r$ for small r . Thus, the probability density function $p_1(U)$ of the velocity generated by a single point vortex is $p_1(U)dU = p(r)dr$, where r is the distance at which the velocity U is found, $r \propto 1/U$. Since $p(r)dr = 2\pi r dr$, one obtains

$$p_1(U) \sim r \left| \frac{dr}{dU} \right| \sim \frac{1}{U} \left| \frac{dr}{dU} \right| \sim \frac{1}{U^3}.$$

In a system of N randomly placed point vortices, the velocity at a point is given by the sum of the contributions of N vortices. For $N \rightarrow \infty$, the central limit theorem ensures asymptotic convergence to a Gaussian, but this convergence is extremely slow.³⁻⁵ Even for a system of 10^6 point vortices, the deviation from a Gaussian is significant. For a finite number of point vortices, the velocity distribution has a Gaussian central portion at low velocities and non-Gaussian tails at high velocity.

For point vortices, high velocities are related to regions close to the vortices themselves, where the vorticity singularity implies also divergent velocities. In two-dimensional turbulence, however, the area (or *core*) of each vortex is finite and vorticity is not divergent. Intuitively, extended vortices can be thought of as point vortices “dressed” by a shape function with finite support. Inside vortices, the properties of the shape function determine the velocity distribution. Sufficiently far from the vortex center, however, the velocity field induced by the presence of an extended vortex can be approximated by that produced by a point vortex (see Jiménez³ and Min *et al.*⁴ for a study of the velocity pdfs induced by an ensemble of vortices with finite cores).

We can thus consider the velocity field induced by a system of point vortices, eliminating regions that are too close to the singularities and that, for extended vortices, would be dominated by the effects of the shape function (this is equivalent to considering point vortices with finite cores). The size of the core regions is determined by a comparison with the mean size of extended vortices in barotropic turbulence. First, we consider $N = 100$ point vortices with constant circulation $\Gamma_i = 1$ and random positions. The velocity pdfs calculated by avoiding a circular region of radius r_* around

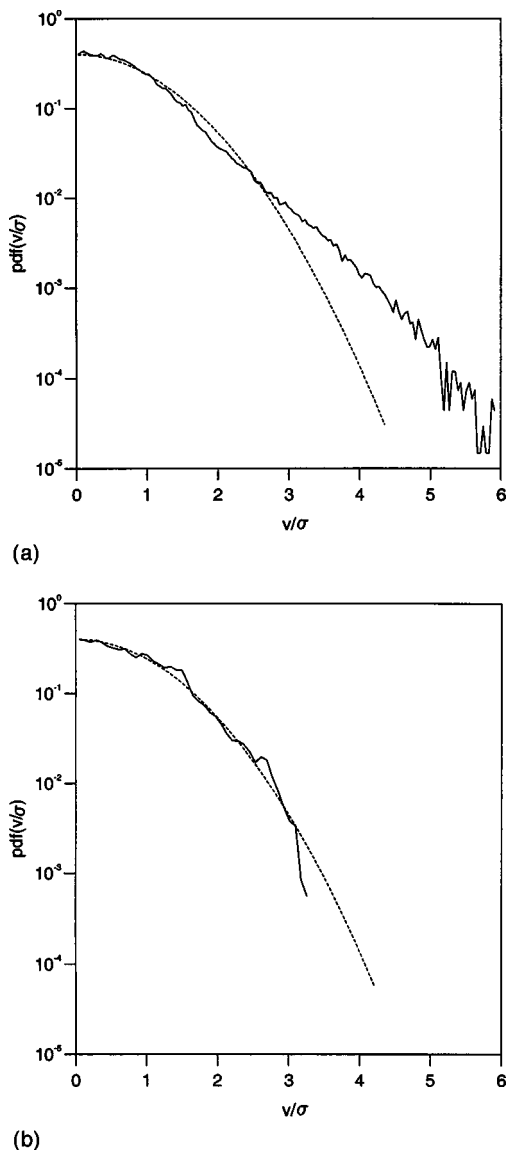


FIG. 9. One-point velocity pdfs obtained from a point-vortex system [Eq. (5)] with $N=100$ vortices with circulation $\Gamma_i=\Gamma_*=1$. Around each point vortex, a circular region of radius $r_*=0.05$ [panel (a)] or $r_*=0.4$ [panel (b)] has been eliminated. The dashed line shows a Gaussian distribution with the same variance of the data.

each vortex are shown in Fig. 9. Panel (a) shows the results for $r_*=0.05$, which is a typical vortex radius in the solution at a higher Reynolds number. In this case, the distribution shows significant non-Gaussian tails at high velocity. Panel (b) refers instead to $r_*=0.4$, which corresponds to the mean radius of the vortex population in the numerical simulation with a narrow-band initial spectrum and $\nu_2=5\times 10^{-7}$ [Fig. 2(b)]. In this case, the distribution is nearly Gaussian.

For a more quantitative comparison, we can consider a configuration where the total number of point vortices and the circulation, position, and size of each of them are equal to the values obtained in the barotropic turbulence solution shown in Fig. 2(a). That is, we approximate each extended vortex with a vorticity singularity with the same position and circulation, and we calculate the instantaneous velocity field induced by the point vortices, avoiding the regions inside the

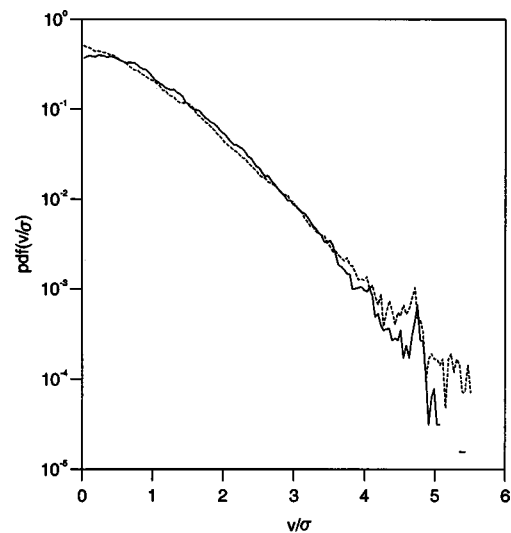


FIG. 10. One-point velocity pdfs obtained from a point-vortex system where the number of vortices, their location, radius, and circulation are as in the turbulent field of Fig. 2(a) (solid line), together with the velocity distribution of the original turbulent field outside vortex cores (dashed line).

areas covered by the extended vortices. The velocity pdfs calculated from the point-vortex system and the original barotropic field are shown in Fig. 10. The two curves are very similar. Since point-vortex systems have zero vorticity between the point singularities, this provides further confirmations that the velocity field in the background of 2-D turbulence is mainly determined by the far field of the vortices.

VI. DISCUSSION AND CONCLUSIONS

In past years, several studies have shown that the dynamics of two-dimensional turbulence can be approximated by the superposition of a finite number of coherent vortices and a random background field. Here, we have shown that the high vorticity concentrations inside coherent structures dominate the velocity field and the properties of particle advection also in the background turbulence between the vortices, and generate non-Gaussian velocity distributions when the Reynolds number is large enough. This is a further indication that most of the statistical properties of 2-D turbulence can indeed be understood by considering the properties of vortex dynamics, resorting, for example, to a point vortex analogy. In an approximate sense, freely decaying two-dimensional turbulence can thus be considered as a “gas of vortices.”

For completeness, in the following we explore the effects of a free surface and of differential rotation on the velocity distributions.

The introduction of a latitudinal variation of the Coriolis parameter leads to a flow with fewer and less intense vortices.^{29,11,30} In turn, this modifies the shape of the velocity pdfs, with a tendency toward approaching a Gaussian distribution as the value of β increases. Figure 11 shows the results obtained for $\beta=10$, and $\nu_2=5\times 10^{-9}$ for narrow-band initial conditions. The two curves refer to the two components u and v of the velocity field that is now anisotropic.

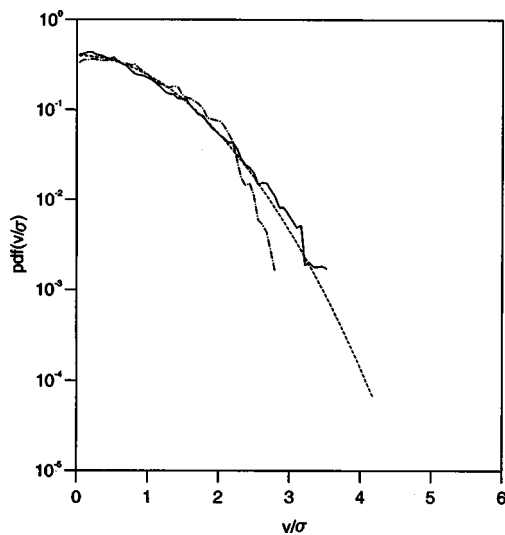
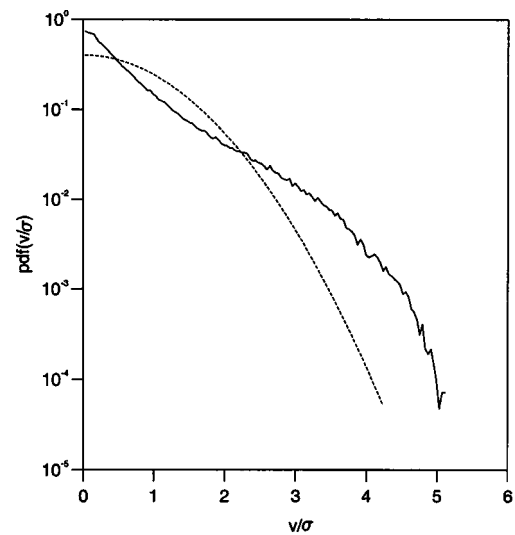


FIG. 11. One-point velocity pdf in a β -plane simulation with narrow-band initial spectrum, $\nu_2=5 \times 10^{-8}$, $1/R=0$, $\beta=10$, and resolution 512×512 collocation points. The two components u (dash-dotted line) and v (full line) of the velocity field are shown separately. The dashed line shows a Gaussian distribution with the same variance.

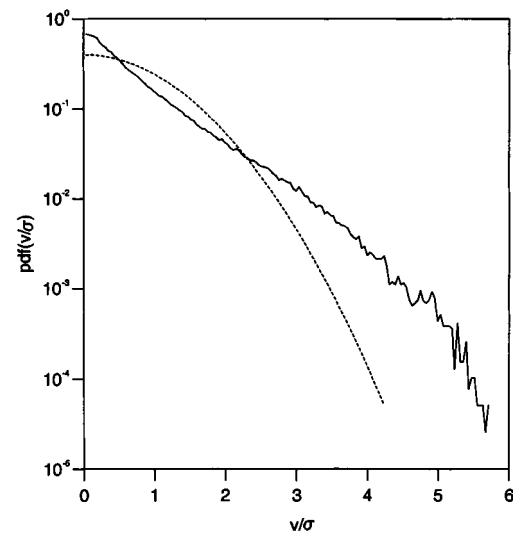
The pdfs are nearly Gaussian, as the field is dominated by Rossby wave “weak” turbulence. Thus, the presence of energetic waves reduces the influence of the vortices on the background field and the non-Gaussianity of the velocity pdfs. Correspondingly, the kinetic energy of the background-induced velocity field is now even larger than that of the vortex-induced velocity field.

Free-surface effects, on the other hand, do not inhibit vortex dominance³¹ and, consequently, do not alter much of the non-Gaussian nature of the velocity pdfs. Figure 12 shows the velocity pdf obtained with $R_0=L/5$ and $\beta=0$. Panel (a) refers to the whole domain, and panel (b) shows the velocity distribution in the background.

Finally, we recall that non-Gaussian velocity pdfs with a shape similar to the one detected here have been observed for subsurface ocean floats in several ocean basins known to be characterized by the presence of intense coherent eddies.⁷ One may then wonder whether the results obtained here can shed light also on the interpretation of oceanic velocity pdfs. Long-lived coherent vortices do indeed permeate the ocean, as indicated by both observations³² and high-resolution numerical simulations.^{33–35} As Smith and Vallis³⁶ have recently discussed, the emerging picture of the world oceans is that of a sea of vortices, where the effects of differential rotation are overcome, at scales smaller than the Rhines scale, by the strongly nonlinear dynamics of geostrophic turbulence with energy concentrated at the scale of the first baroclinic Rossby deformation radius. The results obtained in this work suggest that the non-Gaussian velocity pdfs observed in the ocean could be generated by the dynamics of the coherent eddies, as for the simple case of 2-D turbulence investigated here. Clearly, a full confirmation of this inference can only come from the analysis of experimental data and of high-resolution numerical simulations of the ocean dynamics.



(a)



(b)

FIG. 12. One-point velocity pdf in a simulation with free surface effects, with narrow-band initial spectrum, $\nu_2=5 \times 10^{-8}$, $R=0.2$, $\beta=0$, and resolution 512×512 grid points. Panel (a) shows the velocity distribution of the whole field, panel (b) show the distribution outside vortices. The dashed line indicates a Gaussian distribution with the same variance.

ACKNOWLEDGMENTS

We are grateful to Armando Babiano, Edward A. Spiegel, Massimo Vergassola, and Jeffrey B. Weiss for useful comments on this work.

¹A. S. Monin and A. M. Yaglom, *Statistical Fluid Mechanics* (MIT Press, Cambridge, MA, 1971), p. 769.

²A. Griffa, “Applications of stochastic particle models to oceanographic problems,” in *Stochastic Modelling in Physical Oceanography*, edited by R. J. Adler, P. Muller, and R. B. Rozovskii (Birkhauser, Boston, 1996).

³J. Jiménez, “Probability density in two-dimensional turbulence,” *J. Fluid Mech.* **313**, 223 (1996).

⁴I. A. Min, I. Mézic, and A. Leonard, “Levy stable distributions for velocity and velocity difference in system of vortex elements,” *Phys. Fluids* **8**, 1169 (1996).

⁵J. B. Weiss, A. Provenzale, and J. C. McWilliams, “Lagrangian dynamics in high-dimensional point-vortex systems,” *Phys. Fluids* **10**, 1929 (1998).

⁶T. H. Solomon, E. R. Weeks, and H. L. Swinney, “Observation of anomalous

- lous diffusion and Levy flights in a two-dimensional rotating flow," *Phys. Rev. Lett.* **71**, 3975 (1993).
- ⁷A. Bracco, J. LaCasce, and A. Provenzale, "Velocity pdf's for oceanic floats," *J. Phys. Oceanogr.* **30**, 461 (2000).
- ⁸J. Charney, "Geostrophic turbulence," *J. Atmos. Sci.* **28**, 1087 (1971).
- ⁹D. J. Thomson, "Criteria for the selection of stochastic models of particle trajectories in turbulent flows," *J. Fluid Mech.* **180**, 529 (1987).
- ¹⁰J. Pedlosky, *Geophysical Fluid Dynamics* (Springer-Verlag, New York, 1987), p. 710.
- ¹¹J. C. McWilliams, "The emergence of isolated coherent vortices in turbulent flow," *J. Fluid Mech.* **146**, 21 (1984).
- ¹²P. Tabeling, S. Burkhart, O. Cardoso, and H. Willaime, "Experimental study of freely decaying two-dimensional turbulence," *Phys. Rev. Lett.* **67**, 3772 (1991).
- ¹³A. Provenzale, "Transport by coherent barotropic vortices," *Annu. Rev. Fluid Mech.* **31**, 55 (1999).
- ¹⁴R. Benzi, M. Colella, S. Paternello, P. Santangelo, and A. Vulpiani, "Intermittency and coherent structures in two-dimensional turbulence," *J. Phys. A* **19**, 3771 (1986).
- ¹⁵A. Babiano, C. Basdevant, B. Legras, and R. Sadourny, "Vorticity and passive-scalar dynamics in two-dimensional turbulence," *J. Fluid Mech.* **183**, 379 (1987).
- ¹⁶J. C. McWilliams, "The vortices in two-dimensional turbulence," *J. Fluid Mech.* **219**, 361 (1990).
- ¹⁷M. Farge and T. Philipovitch, "Coherent structure analysis and extraction using wavelets," in *Progress in Wavelet Analysis and Applications*, edited by Y. Meyer and S. Roques (Ed. Frontiers, Gif-sur-Yvette, 1993), p. 477.
- ¹⁸A. Siegel and J. B. Weiss, "A wavelet-packet census algorithm for calculating vortex statistics," *Phys. Fluids* **9**, 1988 (1997).
- ¹⁹M. Farge, K. Schneider, and N. Kevlahan, "Non-Gaussianity and coherent vortex simulation for two-dimensional turbulence using an adaptive orthogonal wavelet basis," *Phys. Fluids* **11**, 2187 (1999).
- ²⁰A. Okubo, "Horizontal dispersion of floatable particles in the vicinity of velocity singularities such as convergences," *Deep-Sea Res.* **17**, 445 (1970).
- ²¹J. B. Weiss, "The dynamics of enstrophy transfer in two-dimensional hydrodynamics," *Physica D* **48**, 273 (1991).
- ²²B. L. Hua and P. Klein, "An exact criterion for the stirring properties of nearly two-dimensional turbulence," *Physica D* **113**, 98 (1998).
- ²³P. Santangelo, R. Benzi, and B. Legras, "The generation of vortices in high-resolution, two-dimensional decaying turbulence and the influence of initial conditions on the breaking of self-similarity," *Phys. Fluids A* **1**, 1027 (1989).
- ²⁴D. Elhmailidi, A. Provenzale, and A. Babiano, "Elementary topology of two-dimensional turbulence from a Lagrangian viewpoint and single-particle dispersion," *J. Fluid Mech.* **257**, 533 (1993).
- ²⁵G. K. Batchelor, *Theory of Homogeneous Turbulence* (Cambridge University Press, Cambridge, 1953), p. 197.
- ²⁶R. Benzi, S. Paternello, and P. Santangelo, "On statistical properties of two-dimensional decaying turbulence," *Europhys. Lett.* **3**, 811 (1987).
- ²⁷H. Aref, "Integrable, chaotic, and turbulent vortex motion in two-dimensional flows," *Annu. Rev. Fluid Mech.* **15**, 534 (1983).
- ²⁸J. B. Weiss and J. C. McWilliams, "Nonergodicity of point vortices," *Phys. Fluids A* **3**, 835 (1991).
- ²⁹P. B. Rhines, "Waves and turbulence on a beta-plane," *J. Fluid Mech.* **69**, 417 (1975).
- ³⁰E. M. Maltrud and G. K. Vallis, "Energy spectra and coherent structures in forced two-dimensional and beta-plane turbulence," *J. Fluid Mech.* **228**, 321 (1991).
- ³¹V. D. Larichev and J. C. McWilliams, "Weakly decaying turbulence in an equivalent-barotropic fluid," *Phys. Fluids A* **3**, 938 (1991).
- ³²D. Stammer, "Global characteristics of ocean variability estimated from regional TOPEX/POSEIDON altimeter measurements," *J. Phys. Oceanogr.* **27**, 1743 (1997).
- ³³E. Chassignet, "Rings in numerical models of ocean general circulation: A statistical study," *J. Geophys. Res.* **97**, 9479 (1992).
- ³⁴A. Paiva, J. Hargrove, E. Chassignet, and R. Bleck, "Turbulent behavior of the fine-mesh (1/12 degree) numerical simulation of the North Atlantic," *J. Mar. Sys.* **21**, 307 (1999).
- ³⁵A. Siegel, J. B. Weiss, J. Toomre, J. McWilliams, P. Berloff, and I. Yavneh, "The quasi-geostrophic dynamics of wind-driven ocean gyres at very high resolution," submitted to *Geophys. Res. Lett.*
- ³⁶K. S. Smith and G. K. Vallis, "The scales and equilibration of mesoscale ocean eddies. Part I: Freely evolving flow," preprint, 2000.